Supplementary Information

Deep Eutectic Solvent-Assisted Recycling of Spent Lithium-Ion Batteries into Electrocatalysts for Polyethylene Terephthalate Upcycling

Xinhui Zhao,* Cheng Kuang, Rujin Zhou, Nina Yang, Chaopeng An, Jing Xu, and Mingyan Wang

Jiangsu Key Laboratory of Function Control Technology for Advanced Materials, School of Environmental and Chemical Engineering, Jiangsu Ocean University, 222005 Lianyungang, Jiangsu, China.

*E-mail: xhzhao@jou.edu.cn

1. Experimental procedures

Raw materials and chemicals

Raw polyethylene terephthalate (PET) was collected from drinking water bottles of Tingyi. Choline chloride ($C_5H_{14}ClNO$, 99%), oxalic acid dihydrate ($C_2H_2O_4{\cdot}2H_2O$, 99.8%), and potassium hydroxide (KOH, 99.99%) were bought from Macklin. Nafion solution (D-520, 5 wt%) was obtained from DuPont. All chemicals were used directly without further purification. Ultrapure water (18 MΩ cm^{-1}) used in the experiments was supplied by a Millipore System (Millipore Q).

Recycling NCM cathode powder

The spent lithium-ion battery was first discharged in 0.5 M NaCl solution for 24 h and then dismantled. After that, the cathode plates were separated and collected. Then, the cathode plates were cut into 1×2 cm^2 pieces and transferred to a tube furnace for calcining at 500 °C for 1 h. The heating rate was 5 ^oC min^{-1}. After the pyrolysis was complete, the electrode material was scraped from the current collector to obtain a complete Al foil and NCM powder.

Extraction of nickel, cobalt, and manganese

DES was simply prepared by mixing choline chloride (27.9 g) and oxalic acid dihydrate (25.2 g) together at a mole ratio of 1:1, followed by stirring at 50 ^oC for 30 min in a flask without any further treatment, obtaining a transparent colorless liquid. The DES was then heated to 120 ^oC with a stirring speed of 400 rpm, and waste NCM powder (0.84 g) was added. The mixture was maintained for 10 h. After leaching, 50 mL of DMSO were introduced into the flask. After 10 min of cooling, Product 2 was separated via vacuum filtration. To the filtrate, 100 mL of water were added, and the mixture was stirred at 70 ^oC for 5 h. Product 4 was then collected by vacuum filtration. The pH of the filtrate was adjusted to 12, and Product 6 was precipitated and separated. Product 2 and Product 4 were calcined at 500 ^oC for 2 h to obtain the corresponding metal oxides, NiO (Product 7) and Co_3O_4 (Product 8), respectively. Mn_3O_4 (Product 9) was obtained by calcining Product 5 at 800 ^oC for 2 h.

Pretreatment of plastics

Alkaline hydrolysis was carried out for depolymerization of PET waste. 1.155 g PET bottle flakes were firstly washed with ethanol and deionized water, respectively. Then, the dried flakes

were added to 60 mL of 1.0 M KOH solution and transferred to a 100 mL Teflon-lined autoclave, which was sealed and maintained at 180 ^{o}C for 4 h. After cooling to room temperature, the resulting solution containing ethylene glycol and terephthalate after filtering was used as the electrolyte for electrochemical test and analysis.

Characterizations

The Fourier-transform infrared spectroscopy (FTIR) experiments were obtained on a IR Prestige-21 from Shimadzu in the range of 500 to 4500 cm^{-1}. Solution ^{1}H NMR experiments were performed on a Bruker-DRX 600 MHz. The chemical shift data were later processed by the MestReNova Program. The X-rays powder diffraction (XRD) patterns of the samples were recorded on an X-rays diffractometer (Rigaku Ultima IV) using Cu Kα as X-rays radiation (λ = 1.5418 Å) under 40 kV and 30 mA. Data were collected in Bragg-Brentano mode using 0.02° divergence with a scan rate of 5° min^{-1}. Scanning electron microscope (SEM) images of the samples were acquired using a ZEISS Sigma 300 scanning electron microscope operated at 3.0 kV. X-rays photoelectron spectroscopy (XPS) was performed on the Thermo Scientific K-Alpha. Typically, the hydrocarbon C1s line at 284.8 eV from adventitious carbon is used for energy referencing in XPS experiments.

Electrochemical measurements

All electrochemical experiments were conducted on CHI 760E electrochemical workstation at room temperature with a working electrode, a Pt gauze (1×1 cm^2) counter electrode, and an Hg/HgO reference electrode. The potentials were converted to reversible hydrogen electrode (RHE) using E(RHE) = E(Hg/HgO) + 0.098 V + 0.059*pH. LSV data were collected for 90% *iR* drop compensation. Chronopotentionmetry test was carried out under the same experimental setup without the *iR* drop compensation. To minimize experimental errors and ensure reproducibility, each electrolysis experiment was repeated three times, and the results were averaged. Electrochemical impedance spectra (EIS) experiments were performed in a frequency range from 0.1 to 10^4 Hz with a perturbation of 5 mV. The explicit Nyquist plots were obtained based on the EIS data.

Product analysis

The liqulid products were analyzed by nuclear magnetic resonance (NMR) spectrometer. ^{1}H

NMR spectra were recorded on a Bruker-DRX 400 MHz NMR spectrometer. The NMR samples were prepared by mixing 0.5 mL of electrolyte with 0.1 mL of D_2O, and 0.1 mL of DMSO aqueous solution (internal standard). The DMSO solution was prepared by diluting 5 μL of DMSO in 10 mL of deionized water. The concentration of product was quantitatively determined from its NMR peak area relative to that of the internal standard using the calibration curve, which was obtained from a series of standard HCOOH solutions (Figure 20).

The Faradaic efficiency (FE) was calculated with the following equations:

$$\mathrm{FE} = 100\% \times \frac{\text{mole of produced formate}}{\text{total charge passed} \;/\; (\mathrm{n} \times 96485\,\mathrm{C} \cdot \mathrm{mol}^{-1})}$$

where n = 3 is the number of electron transfer for formate; 96485 $C \cdot mol^{-1}$ is the Faraday constant.

2. Results and discussion

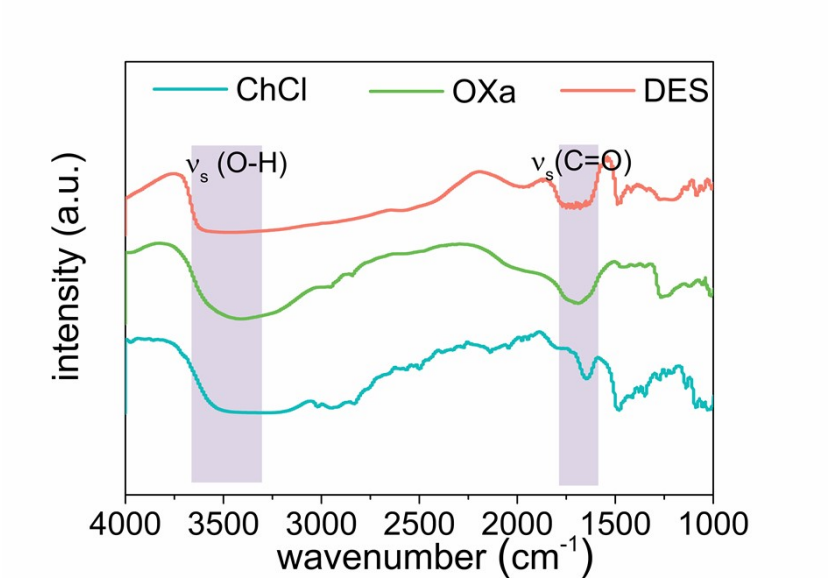

Figure S1. FT-IR analysis of the DES, ChCl, and OxA. The DES still retains the original feature peaks of each component, except for the obvious shift to the left at 3602 cm^{-1}, which shifts from 3332 cm^{-1} in ChCl and 3643 cm^{-1} in OxA. The result indicates the formation of hydrogen bonds between ChCl and OxA. A blue-shift of the C=O vibration from 1676 cm^{-1} in OxA to 1722 cm^{-1} in DES is also observed due to the strong electronegativity of Cl^- and the induction effect.[1]

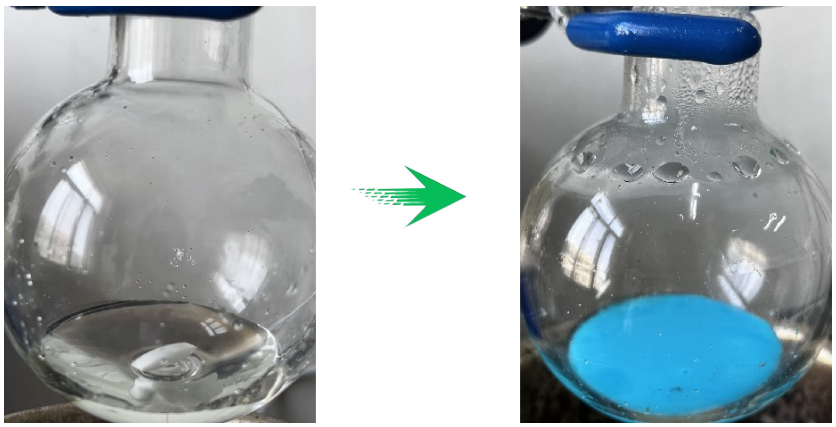

Figure S2. Photograph of DES before (left) and after (right) adding NCM materials (right).

Separation and characterization of nickel

To better understand the dissolution and separation mechanism, several characterizations were performed to determine the products. As depicted in Figure S3a, the precipitate formed after leaching (Product 2) is confirmed to be $NiC_2O_4{\cdot}2H_2O$, as verified by the XRD results. Additionally, FT-IR was conducted to investigate the composition of Product 2 (Figure S3b). The FT-IR spectrum of Product 2 exhibits prominent peaks around 3400 cm^{-1} (O-H stretching), 1615 cm^{-1} (C=O antisymmetric stretching), 1358 and 1310 cm^{-1} (C-O symmetric stretching), which are consistent well with the characteristic features of $NiC_2O_4{\cdot}2H_2O$.[2] To enhance the value of the residue, we calcined Product 2 at 500 °C for 2 h to obtain nickel oxide (Product 7). XRD experiments confirmed that the diffraction peaks of the calcined powder align well with NiO (Figure S4a).[3] X-rays photoelectron spectroscopy (XPS) was then performed to elucidate the composition of the calcined powder. As shown in the Ni 2p spectrum (Figure S4b), the peaks at 854.2 and 862.5 eV correspond to Ni $2p_{3/2}$, while the peaks at 871.6 and 879.2 eV are ascribed to Ni $2p_{1/2}$.[4] In the O 1s spectrum (Figure S4c), the peak at 528.9 eV confirms the formation of Ni-O.[5] We further examined the morphology of the obtained NiO using scanning electron microscope (SEM). As shown in Figure S5, NiO presents a nanorod structure with pores. The corresponding energy dispersive spectrometer (EDS) elemental mapping clearly reveals the uniform distribution of Ni and O. These results collectively indicate the successful formation of NiO after the calcination of Product 2.

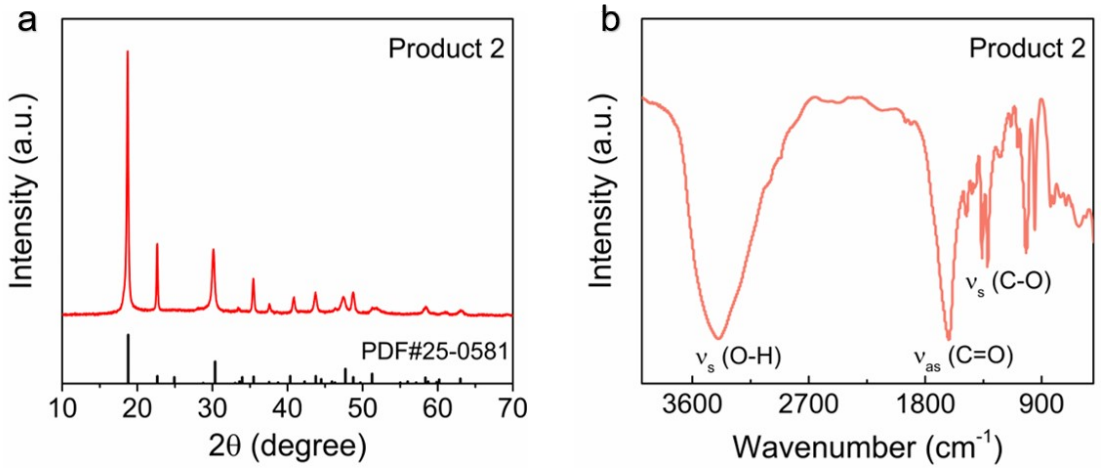

Figure S3. (a) XRD pattern and (b) FT-IR spectrum of Product 2 ($NiC_2O_4{\cdot}2H_2O$).

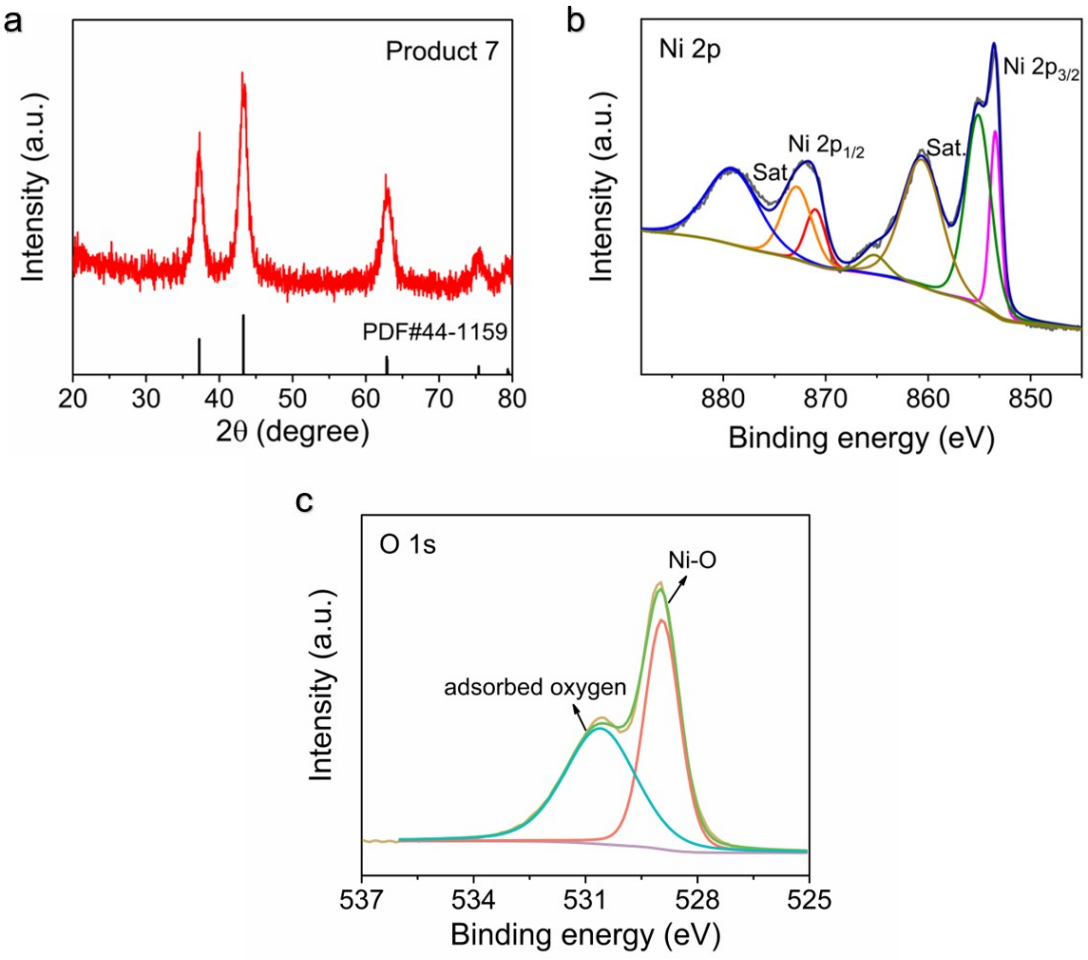

Figure S4. (a) XRD pattern, (b) Ni 2p XPS spectrum, and (c) O 1s XPS spectrum of Product 7 (NiO).

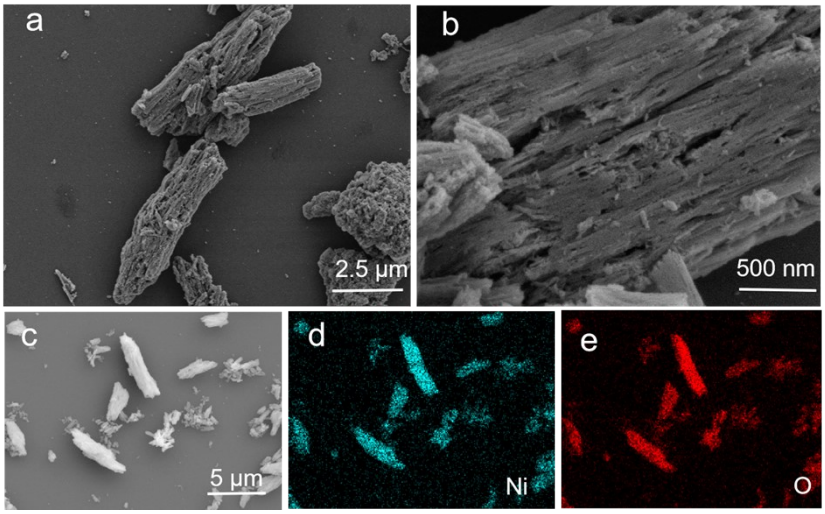

Figure S5. (a-b) SEM images and (c-e) EDS elemental mapping of Product 7 (NiO).

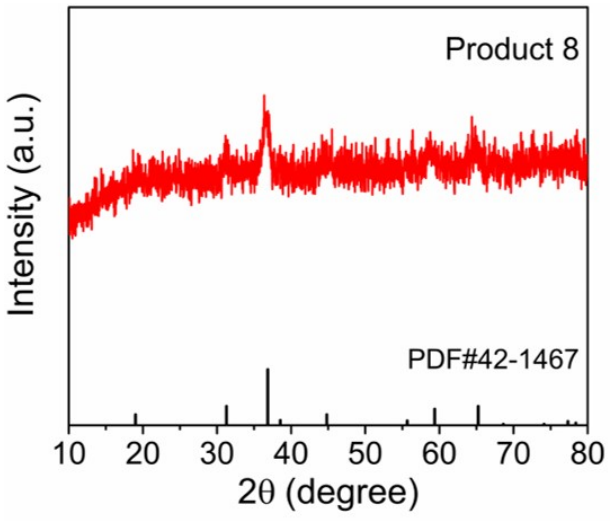

Figure S6. XRD pattern of Product 8 (Co_3O_4).

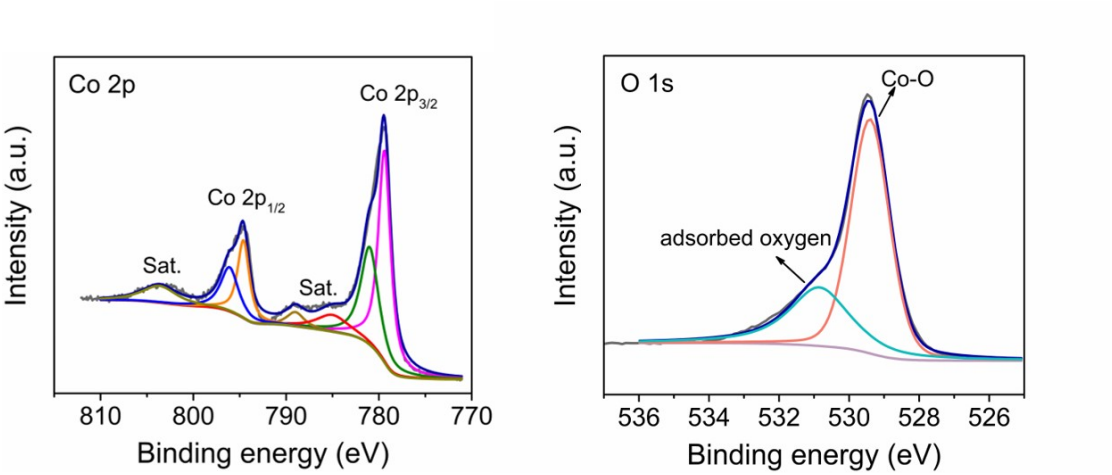

Figure S7. (a) Co 2p and (b) O 1s XPS spectra of Product 8 (Co_3O_4).

Separation and characterization of manganese

After the separation steps, nickel and cobalt were efficiently isolated, while manganese was accumulated in the remaining filtrate (Product 5). Manganese was then separated as manganese hydroxide ($Mn(OH)_2$) precipitation by adjusting the pH value of the filtrate to 12. Since manganese hydroxide is easily oxidized, the resulting precipitate was subsequently converted into a mixture (Product 6) of manganese hydroxide, hydroxyl oxidation-manganese oxide, and manganese dehydrate due to the oxidation by dissolved oxygen in the solution.[6] The obtained Mn-oxide mixture was then calcined at 800 °C for 2 h, resulting in high-purity Mn_3O_4 (Product 9), as confirmed by the XRD pattern (Figure S8).[7] SEM images reveals the formation of a dense Mn_3O_4 nanosheet region (Figure S9a-b). The corresponding EDS mapping visually confirms that the homogeneous distribution of Mn and O elements within the Mn_3O_4 material (Figure S9c-e). An XPS experiment was further performed to analyze the oxidation state of manganese. The high-resolution Mn 2p spectrum shows two peaks at 641.1 and 652.9 eV, indicating the presence of both divalent and trivalent manganese, consistent with the XRD results (Figure S10a). The O 1s XPS spectrum (Figure S10b) also supports these findings, with peaks at 528.9, 530.2, and 531.5 eV, further confirming the presence of Mn_3O_4.[8]

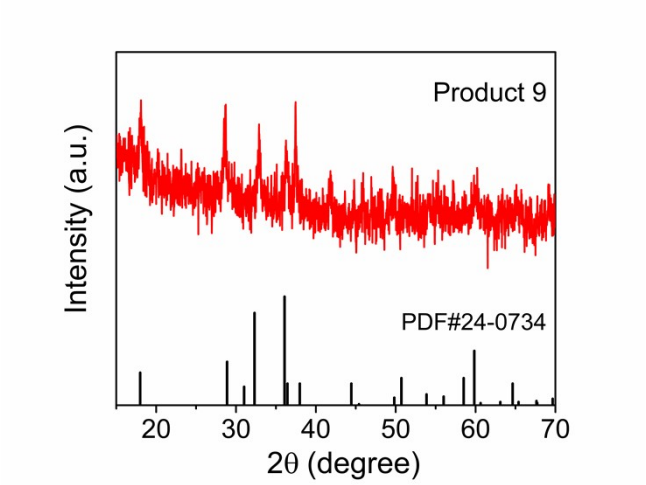

Figure S8. XRD pattern of Product 9 (Mn_3O_4).

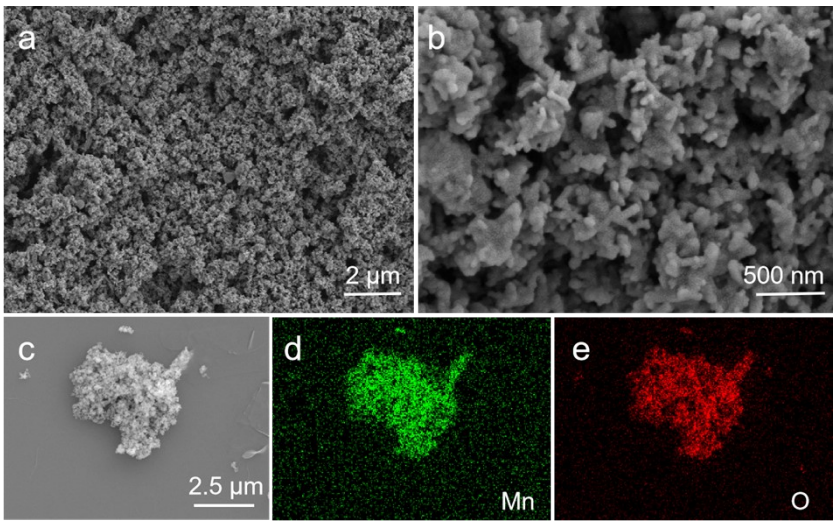

Figure S9. (a-b) SEM images and (c-e) EDS elemental mapping of Product 9 (Mn_3O_4).

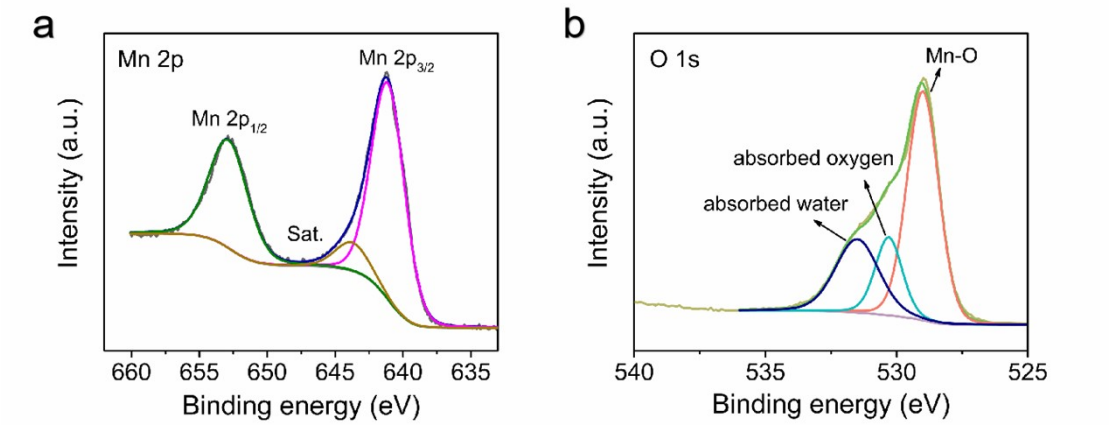

Figure S10. (a) Mn 2p and (b) O 1s XPS spectra of Product 9 (Mn_3O_4).

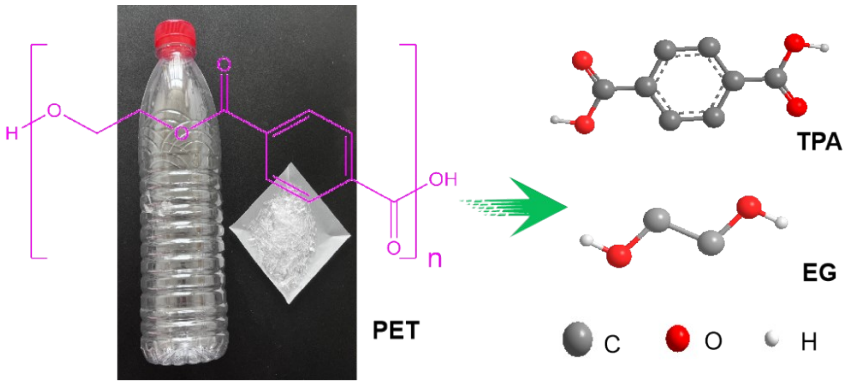

Figure S11. PET hydrolysis diagram.

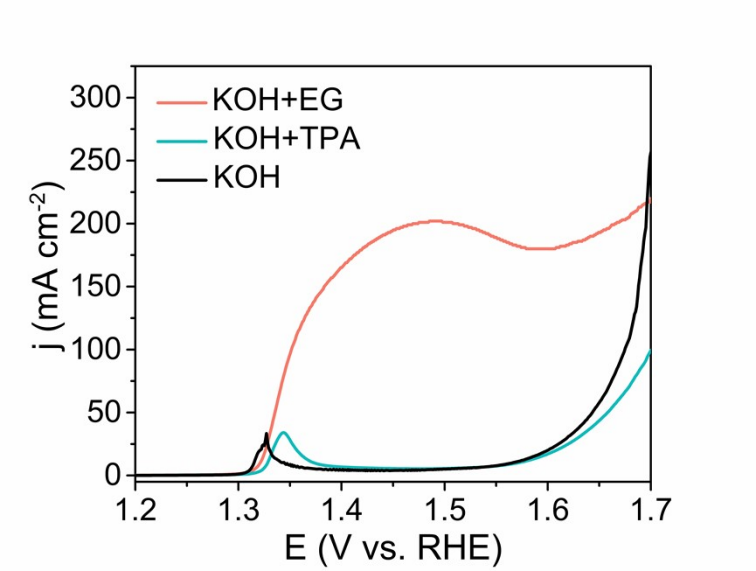

Figure S12. LSV curves of the Co_3O_4 catalyst in blank 1.0 M KOH solution, 1.0 M KOH solution with 0.1 M TPA and 0.1 M EG.

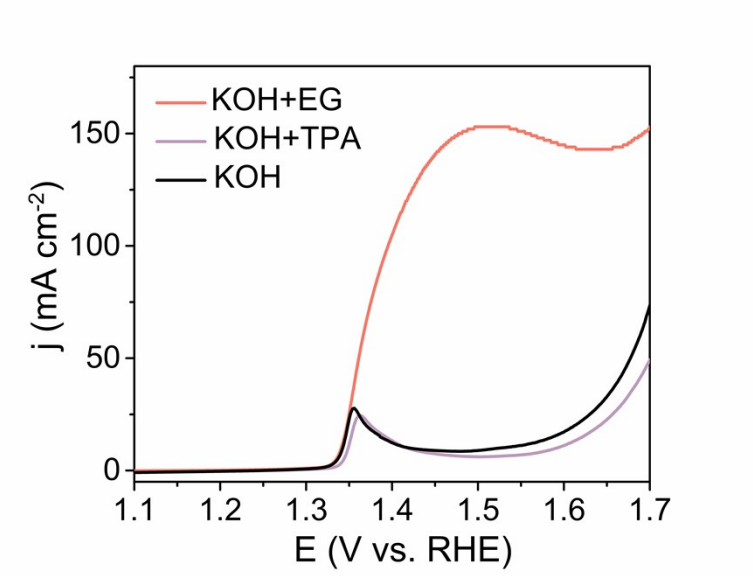

Figure S13. LSV curves of the NiO catalyst in blank 1.0 M KOH solution, 1.0 M KOH solution with 0.1 M TPA and 0.1 M EG.

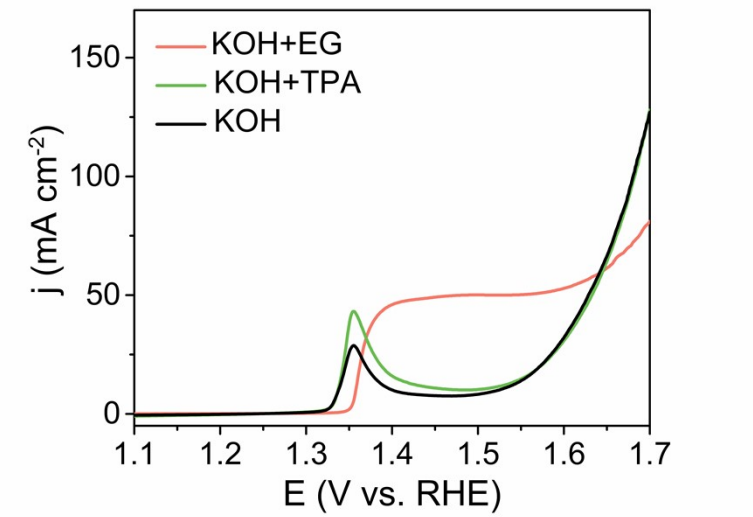

Figure S14. LSV curves of the Mn_3O_4 catalyst in blank 1.0 M KOH solution, 1.0 M KOH solution with 0.1 M TPA and 0.1 M EG.

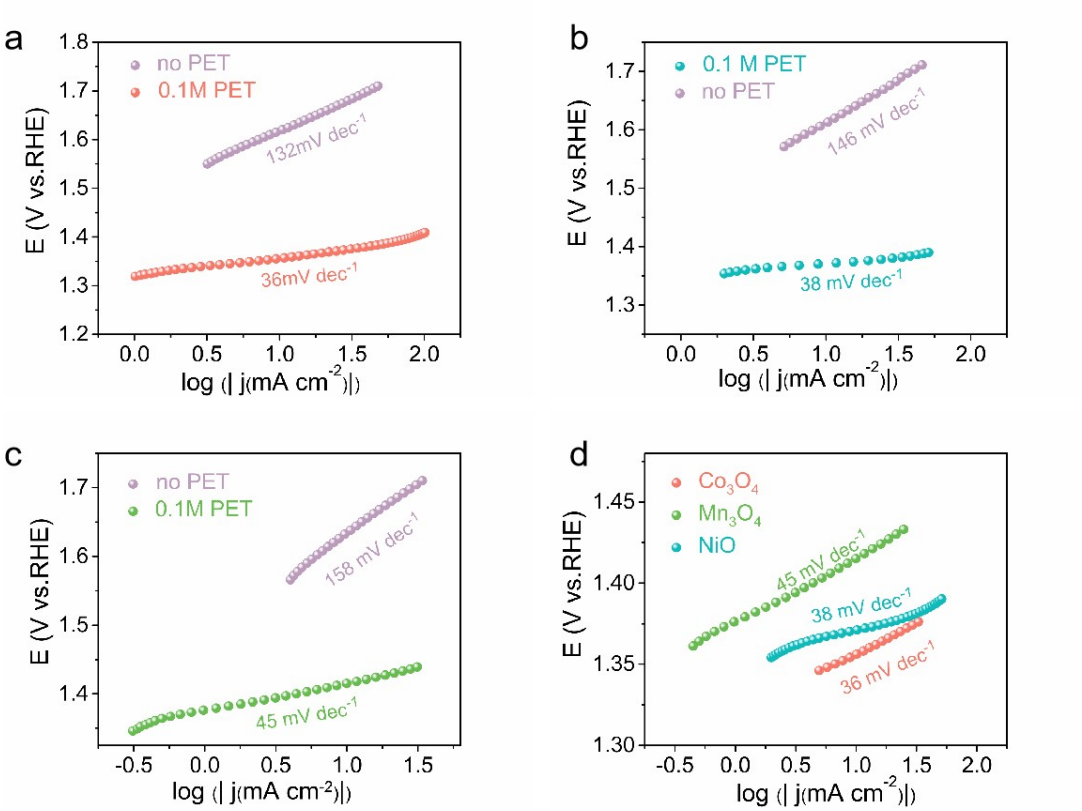

Figure S15. Tafel plots for (a) Co_3O_4, (b) NiO, and (c) Mn_3O_4 catalysts in 1.0 M KOH with or without 0.1 M PET hydrolysate. (d) The comparison of Tafel plots for the three catalysts in PET hydrolysate.

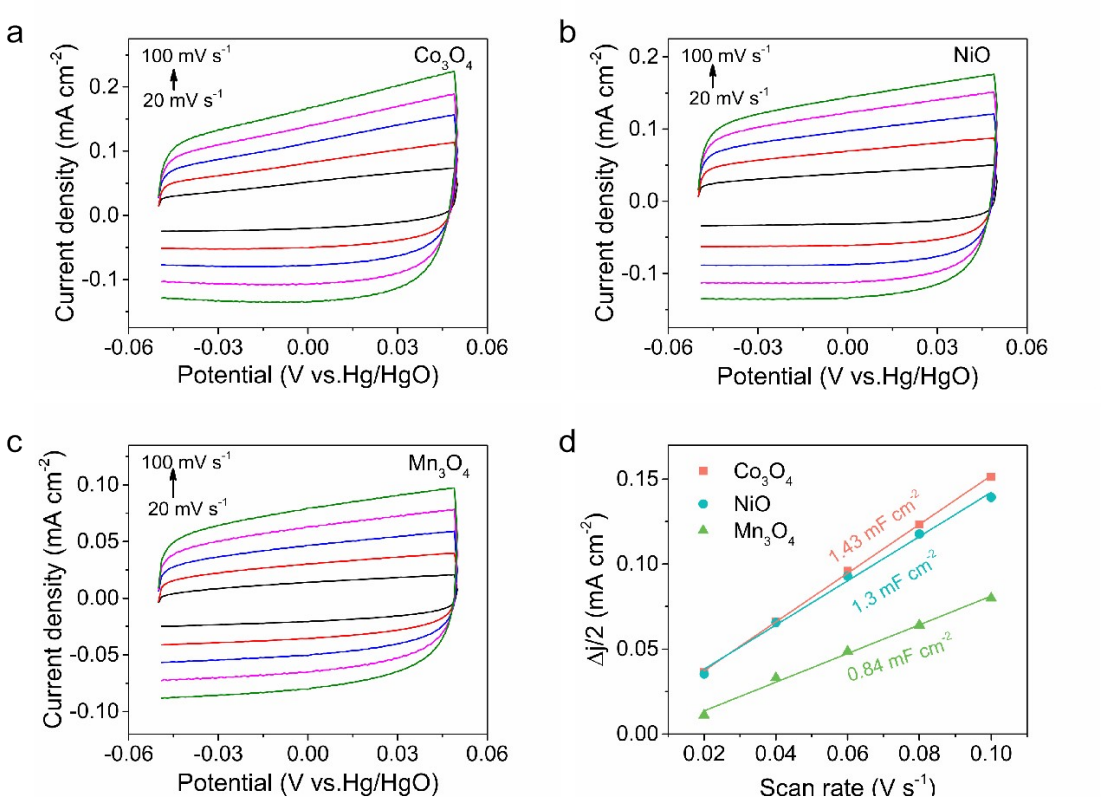

Figure S16. (a) CV curves of (a) Co_3O_4, (b) NiO, and (c) Mn_3O_4 in 1 M KOH with 0.1 M PET hydrolysate. (d) The corresponding double layer capacitance (C_{dl}) values of the samples.

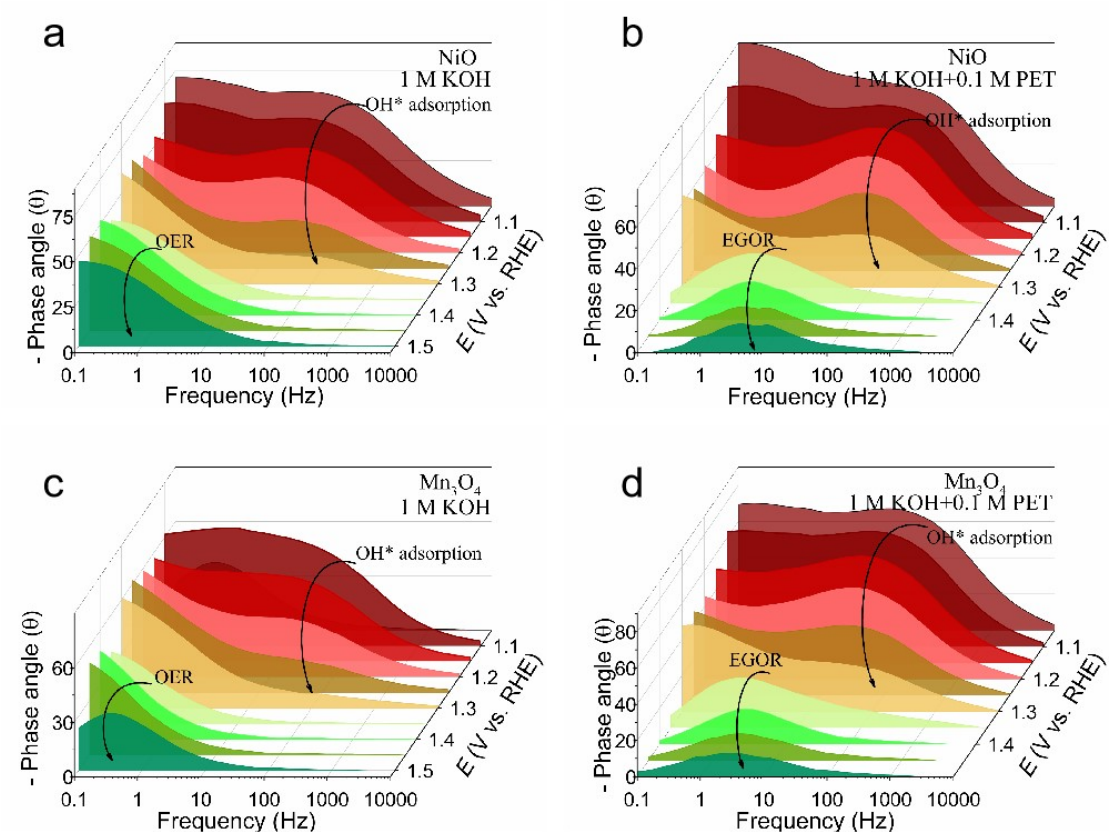

Figure S17. Bode phase plots of the in-situ EIS on (a-b) NiO and (c-d) Mn_3O_4 catalysts.

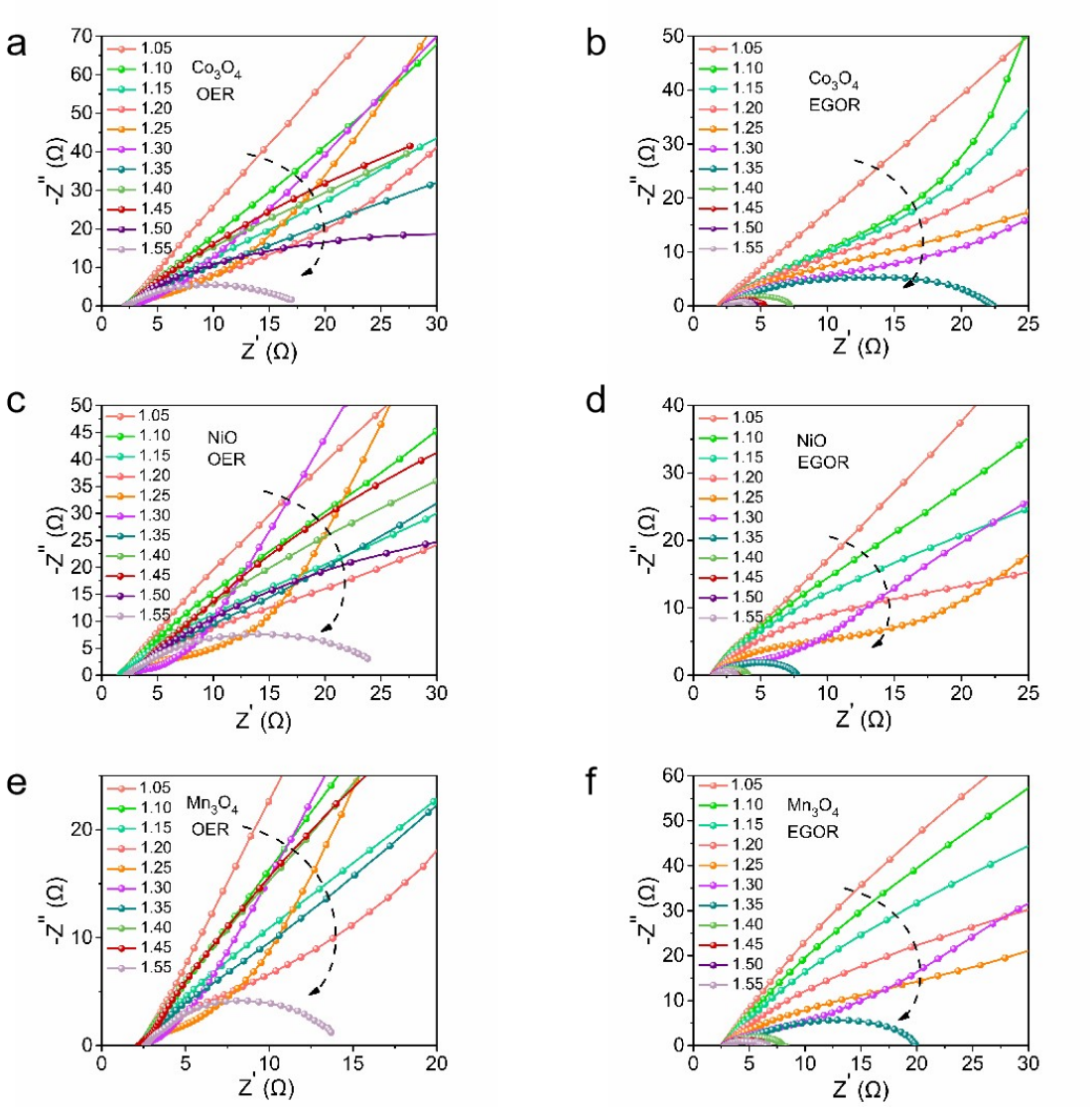

Figure S18. Nyquist plots of the three catalysts at various potentials.

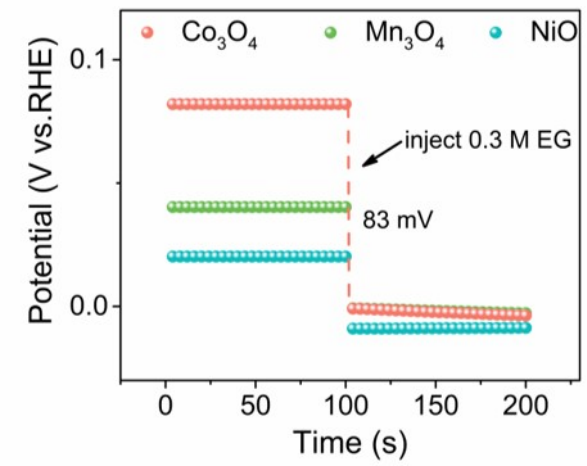

Figure S19. OCP curves of NiO, Co_3O_4, and Mn_3O_4 catalysts in 1.0 M KOH before and after 0.3 M EG was added.

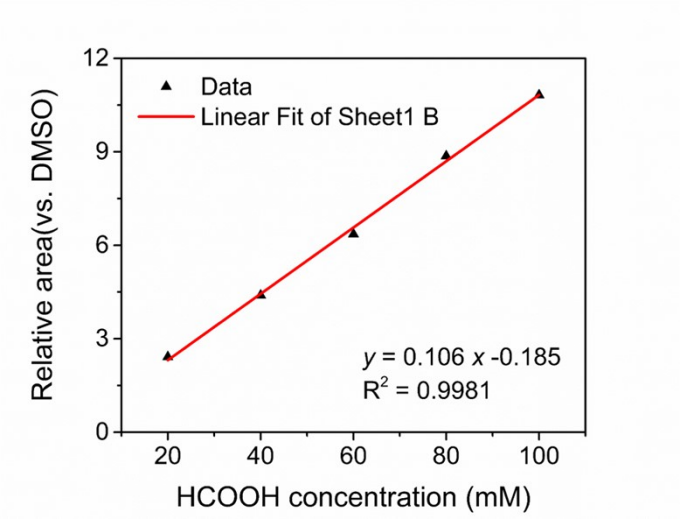

Figure S20. Calibration curves of formic acid in 1 M KOH.

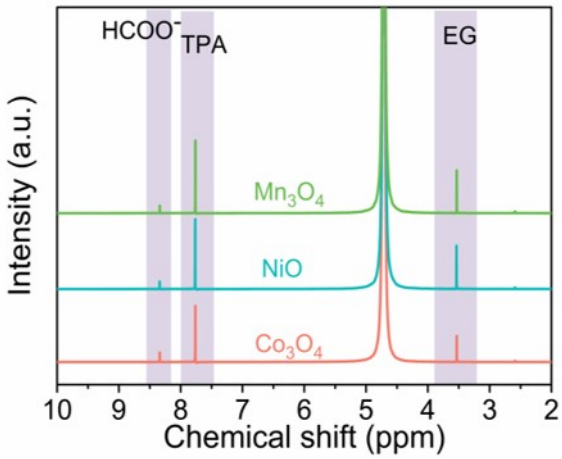

Figure S21. ^{1}H NMR spectra of the electrolyte after electrolysis on the three catalysts.

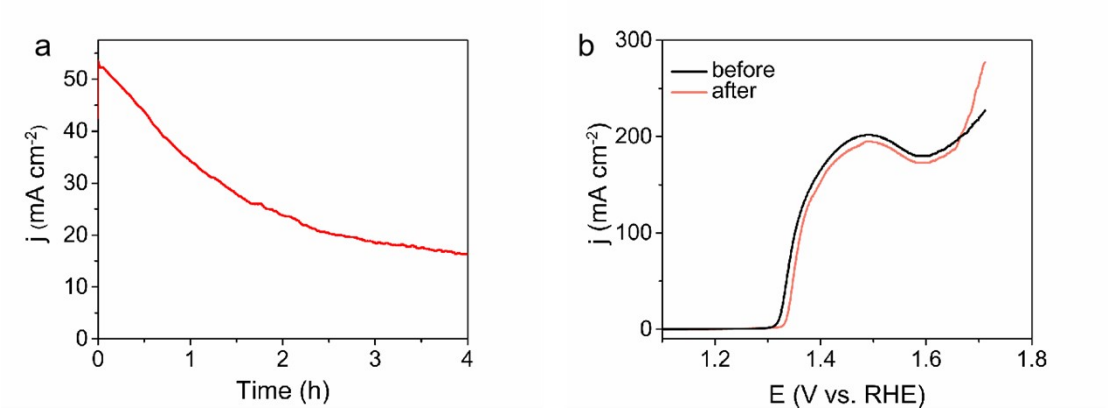

Figure S22. (a) Chronoamperometric electrolysis of the Co_3O_4 catalyst at 1.52 V vs. RHE for continuous 4 h electrolysis. (b) LSV curves before and after 4 h electrolysis.

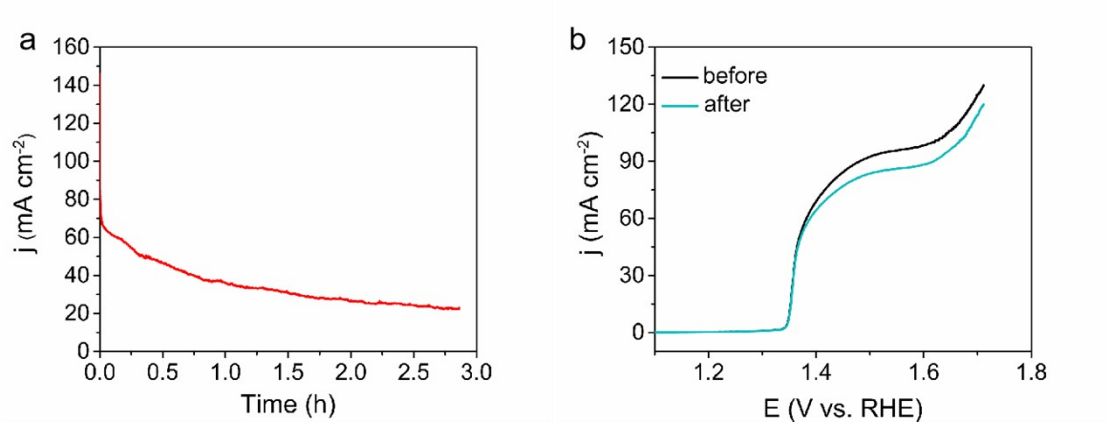

Figure S23. (a) Chronoamperometric electrolysis of the NiO catalyst at 1.52 V vs. RHE for continuous 2 h electrolysis. (b) LSV curves before and after 2 h electrolysis.

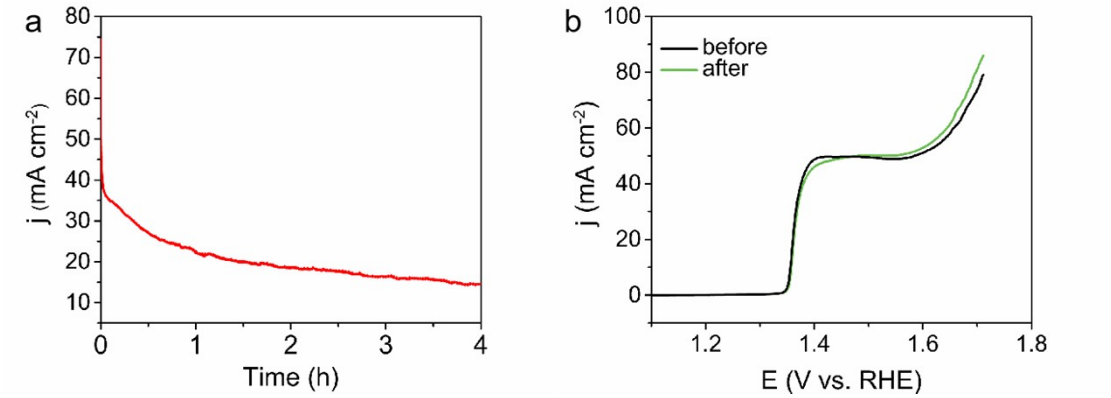

Figure S24. (a) Chronoamperometric electrolysis of the Mn_3O_4 catalyst at 1.52 V vs. RHE for continuous 4 h electrolysis. (b) LSV curves before and after 4 h electrolysis.

Reference

1. R. Gautam, N. Kumar and J. G. Lynam, *J. Mol. Struct.*, 2020, **1222**, 128849.
2. A. N. Puzan, V. N. Baumer, D. V. Lisovytskiy and P. V. Mateychenko, *J. Solid State Chem.*, 2018, **266**, 133-142.
3. M. Wang, N. Zhang, Y. Feng, Z. Hu, Q. Shao and X. Huang, *Angew. Chem. Int. Ed.*, 2020, **59**, 14373-14377.
4. S. Ghosh, B. Dasgupta, S. Kalra, M. L. P. Ashton, R. Yang, C. J. Kueppers, S. Gok, E. G. Alonso, J. Schmidt, K. Laun, I. Zebger, C. Walter, M. Driess and P. W. Menezes, *Small*, 2023, **19**, e2206679.
5. X. Zhao, C. Kuang, C. An and M. Wang, *Chem. Eng. J.*, 2024, **500**, 157275.
6. R. M. Mc Kenzie, in *Miner. Soil Environ.*, 1989, DOI: https://doi.org/10.2136/sssabookser1.2ed.c9, pp. 439-465.
7. X. Li, P. F. Liu, L. Zhang, M. Y. Zu, Y. X. Yang and H. G. Yang, *Chem. Commun.*, 2016, **52**, 10566-10569.
8. Y. Zhang, N. Cao, H. Cheng, X. Zhao, L. Qiu, Y. Fang, J. Liao, X. Cai, X. Tian, L. Lei, P. Xie and X. Zhang, *Appl. Catal., B*, 2024, **355**, 124171.